Colloids and Surfaces A: Physicochemical and Engineering Aspects 727 (2025) 138212

Contents lists available at ScienceDirect

Colloids and Surfaces A: Physicochemical and Engineering Aspects

journal homepage: www.elsevier.com/locate/colsurfa

A sustainable approach to water purification: Strontium-modified ZnO nanoparticles for UV/sunlight-driven degradation and antibacterial disinfection

V. Mariyappillai [a], C. Shiyamala [a,*], M. Tiffany [b], T. Abisheik [b], V. Pandiyan [b,*], Abdullah K. Alanazi [c], Parvathalu Kalakonda [d], Arun Thirumurugan [e], Gabriela Sandoval-Hevia [f], Krishnakumar Balu [g,h,**]

[a] PG & Research Department of Chemistry, Thiru Kolanjiappar Govt. Arts College (Affiliated to Annamalai University), Vriddhachalam, Tamil Nadu 606001, India
[b] Department of Physics, Nehru Memorial College (Autonomous), Affiliated to Bharathidasan University, Puthanampatti, Tiruchirappalli, Tamil Nadu 621007, India
[c] Department of Chemistry, College of Science, Taif University, P.O. Box 11099, Taif 21944, Saudi Arabia
[d] Department of Physics, Smart Nanomaterial Research Laboratory, Government City PG College (A), Osmania University, Hyderabad, Telangana 500002, India
[e] Sede Vallenar, Universidad de Atacama, Av. Costanera #105, Vallenar 1612178, Chile
[f] Departamento de Química, Facultad de Ciencias Naturales, Matemáticas y del Medio Ambiente, Universidad Tecnológica Metropolitana, Las Palmeras 3360, Ñuñoa, Región Metropolitana 7800003, Chile
[g] Saveetha School of Engineering, Saveetha Institute of Medical and Technical Sciences (SIMATS), Chennai, Tamil Nadu 602105, India
[h] Department of Civil Engineering, Yeungnam University, Gyeongsan 38541, Republic of Korea

HIGHLIGHTS

- Sr-doped and undoped ZnO were prepared successfully.
- 3 wt% Sr-ZnO showed ≈100 % RR 120 degradation under UV-A and sunlight irradiation.
- Sr-ZnO showed excellent antimicrobial activity against both Gram ± bacteria.

GRAPHICAL ABSTRACT

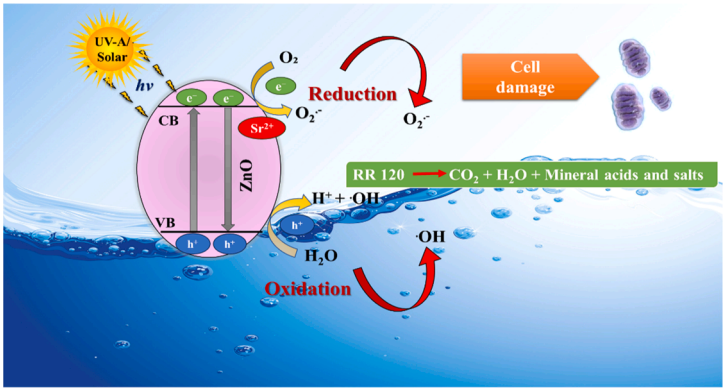

ARTICLE INFO

Keywords:
Sr-ZnO
Photocatalysis
Reactive Red 120

ABSTRACT

The escalating challenge of water contamination by persistent organic pollutants needs the development of effective and long-lasting cleanup strategies. To improve photocatalytic and antibacterial performance, this study detailed the synthesis of pure and strontium-loaded zinc oxide (Sr-ZnO) nanoparticles using a simple co-precipitation approach. Structural, morphological, and optical characterizations employing XRD, FT-IR,

* Corresponding authors.
** Corresponding author at: Saveetha School of Engineering, Saveetha Institute of Medical and Technical Sciences (SIMATS), Chennai, Tamil Nadu 602105, India.
E-mail addresses: cshiyamala@rediffmail.com (C. Shiyamala), pandiyanphy@gmail.com (V. Pandiyan), kbalu@us.es (K. Balu).

https://doi.org/10.1016/j.colsurfa.2025.138212
Received 12 July 2025; Received in revised form 11 August 2025; Accepted 27 August 2025
Available online 28 August 2025
0927-7757/© 2025 Elsevier B.V. All rights are reserved, including those for text and data mining, AI training, and similar technologies.

Antibacterial activity
UV-A and sunlight degradation

Raman, PL, UV-DRS, FE-SEM, HR-TEM, EDS, and XPS demonstrated effective Sr^{2+} integration into the ZnO lattice without altering the wurtzite structure. Among the various loading doses, 3 wt% Sr-ZnO demonstrated the most efficient photocatalytic activity, attaining ≈ 100 % degradation of Reactive Red 120 (RR 120) dye under UV-A irradiation in 30 min and ≈ 100 % degradation under sunlight within 50 min. Improved charge carrier separation, longer light absorption, and enhanced reactive oxygen species (ROS) formation all contributed to improved performance. Optimal dye degradation occurred at neutral pH and a catalyst dose of 50 mg. Reusability testing revealed that after numerous cycles, efficiency exceeded 90 %. In addition to photocatalytic applications, 3 wt% Sr-ZnO was examined for antibacterial efficacy against *Staphylococcus aureus, Pseudomonas aeruginosa, Bacillus subtilis,* and *Escherichia coli* and showed significant bactericidal activity. Overall, the study establishes Sr-loaded ZnO, particularly at 3 wt% loading, as a highly efficient, stable, and environmentally acceptable nanomaterial for dye degradation and microbial disinfection. These findings highlight its enormous potential for integrated wastewater treatment systems, which provide a long-term solution for reducing chemical and biological contaminants in aquatic ecosystems.

1. Introduction

Soaring urban development and the demand for manufacturing growth, spurred by expanding global populations, have made a considerable contribution to environmental degradation, notably water contamination [1]. Manufacturing industry effluents, agricultural runoff, home waste, mining operations, and oil spills all contribute harmful contaminants into aquatic habitats [2]. These pollutants endanger biodiversity and disrupt the biological equilibrium of aquatic life [3]. Among these contaminants, textile dyes are the most significant contribution. Although synthetic dyes are essential in industries such as fashion and textiles due to their brilliant and long-lasting colouring capabilities, they are chemically stable and very toxic even at low doses [4]. Their intricate molecular architectures, which include aromatic rings and azo linkages, render them resistant to natural destruction [5]. As a result, these colours remain in water bodies, reducing light penetration, disrupting photosynthesis [6], and having serious environmental implications. In addition to environmental damage, chronic exposure to dye-contaminated water can have major health consequences for humans, including an increased risk of cancer, reproductive difficulties, and developmental issues [7]. Alarmingly, a recent study indicated that over 3.2 million people perish each year as a result of drinking contaminated water, emphasising the critical need for more effective water treatment solutions [8]. Conventional procedures such as coagulation, flocculation, adsorption, and biological treatments are frequently insufficient for complete removal of synthetic dyes. These procedures often result in pollutant phase transfer rather than degradation, which produces secondary waste. Furthermore, the chemical robustness of dyes restricts the efficacy of biological therapies. To solve these issues, semiconductor-based photocatalysis has emerged as a viable option [9]. This approach uses light energy to activate semiconductor materials, which can convert organic contaminants into innocuous byproducts such as water and carbon dioxide [10]. Zinc oxide (ZnO) has received a lot of attention among photocatalysts because of its many advantages, including low cost, environmental friendliness, high photosensitivity, ease of synthesis, and strong oxidative capabilities [11, 12].

Zinc oxide (ZnO) is an extensively studied semiconductor material that has received a lot of attention recently due to its outstanding optical, chemical, and electrical properties [13,14]. It is an II-VI semiconductor with a large direct band gap of 3.37 eV and a high exciton binding energy of 60 meV, allowing for substantial ultraviolet (UV) light absorption. ZnO is environmentally safe, non-toxic, thermally stable, and cost-effective, making it ideal for various applications, including sensors, solar cells, light-emitting diodes, and photocatalysis [15]. ZnO has shown considerable potential as a photocatalyst for environmental remediation, particularly in the breakdown of organic contaminants such as synthetic dyes found in industrial wastewater [16–18]. When exposed to UV light, ZnO produces reactive oxygen species (ROS), which can degrade complicated colour molecules into harmless byproducts [19]. Pure ZnO's photocatalytic effectiveness is restricted by its inability to use visible light and the quick recombination of photogenerated electron-hole pairs [20]. To improve its performance, several tactics, including loading, composite creation, and surface modification, have been investigated. These efforts aim to improve light absorption, charge carrier separation, and overall catalytic activity, establishing ZnO as an important material in the development of sustainable water purification systems [21–23].

According to prior research, Jan et al., [24] investigated the hydrothermal production of both zinc oxide and strontium-loaded zinc oxide nanoparticles. UV, FTIR, SEM, XRD, and EDX analysis verified the presence of strontium in the ZnO nanoparticles. The optical band gaps were discovered to be 3.16 eV for ZnO and 2.90 eV for Sr-ZnO nanoparticles. Unloaded ZnO nanoparticles had better photocatalytic activity than strontium-loaded counterparts in the breakdown of Acid Violet 17 dye. The degradation rate was regulated by the irradiation period, dye concentration, catalyst weight, and pH. Kumaran et al., [25] explore the photocatalytic activity of zinc oxide and strontium-loaded ZnO nanoparticles, evaluating their efficacy in photocatalytic oxidation of methyl orange and methylene blue. The study shows that strontium loading greatly improves ZnO's photocatalytic performance when compared to pure ZnO. The best results were obtained with a Sr/Zn mole ratio of 1:2, calcined at 600°C for 7 h. The study also found that cationic methylene blue degrades more quickly than anionic methyl orange, possibly due to higher negative charge accumulation on the catalyst surface. Agale et al., [26] employ the hydrothermal approach to synthesise and characterise strontium-loaded zinc oxide hierarchical hexagonal nano discs. To characterise the synthesised materials, various techniques were used, including XRD, FTIR, UV, FESEM, EDAX, TEM, and XPS. The paper focuses on the successful loading of strontium in ZnO, which was confirmed by X-ray diffraction examinations. The synthesised catalyst displayed outstanding photocatalytic activity in wastewater treatment, specifically the photodegradation of methylene blue dye. The greatest results were obtained with a 5 wt% Sr-loaded ZnO catalyst, which had an impressive degradation rate constant k of up to 0.0389 min^{-1} . Although several Sr-ZnO-based photocatalysts have been reported, few studies have optimized Sr doping levels to maximize sunlight-driven degradation efficiency while maintaining structural stability. Our study introduces a tailored Sr-ZnO composition that achieves this balance, offering improved reusability and photocatalytic efficiency.

Building on ZnO's photocatalytic potential, strontium-loaded zinc oxide (Sr-ZnO) has emerged as a promising modification technique for overcoming its inherent limits. Loading ZnO with strontium (Sr^{2+}), an alkaline earth metal with a slightly greater ionic radius than Zn^{2+}, introduces lattice distortions and defect sites, significantly modulating its structural and electrical properties [27]. These improvements result in improved charge separation and reduced recombination of photogenerated electron-hole pairs, considerably increasing photocatalytic efficiency. Furthermore, Sr loading can extend ZnO's light absorption range into the visible region by reducing the band gap or introducing mid-gap states, allowing for greater solar spectrum utilisation [28]. This improvement renders Sr-ZnO especially effective in degrading persistent

organic pollutants like synthetic dyes when exposed to the sun or visible light. Furthermore, Sr inclusion can alter the surface morphology of ZnO and increase its specific surface area, resulting in additional active sites for photocatalytic processes. As a result, Sr-ZnO nanostructures outperformed virgin ZnO in terms of photocatalytic activity, providing a more efficient and sustainable method of water purification and environmental remediation. The synergistic effects of Sr loading offer up new avenues for optimising ZnO-based photocatalysts for enhanced wastewater treatment techniques [29].

This research focuses on synthesising and analysing pure and strontium-loaded ZnO nanoparticles to improve their structural, optical, and photocatalytic properties. Various techniques were used for comprehensive characterisation, including FE-SEM and HR-TEM for surface morphology, XRD for crystal structure, and FT-IR, FT-Raman, and XPS for identifying functional groups and bonds. PL and UV-DRS investigated optical behaviour such as band gap energy and charge carrier dynamics. The photocatalytic efficiency of Reactive Red 120 dye was tested under UV and sunlight, monitored using UV-Vis spectroscopy. Strontium loading enhanced photocatalytic activity, which was attributed to improved charge carrier separation, stability, and light absorption. Aside from photocatalytic degradation, gas chromatography-mass spectrometry (GC-MS) was used to identify intermediate chemicals, offering vital insights into the dye's breakdown route. Reusability tests revealed that the Sr-loaded ZnO nanoparticles were long-lasting, with just a minor decrease in photocatalytic efficacy between cycles. Furthermore, trapping studies were carried out to identify the essential reactive species involved in the degradation mechanism, such as hydroxyl radicals, superoxide radicals, and photogenerated holes, resulting in a better understanding of the photocatalytic process. These findings point to a high potential for strontium-loaded ZnO nanoparticles in applications such as environmental remediation, optoelectronics, and antimicrobial treatments.

2. Experimental setup

2.1. Synthesis of Sr loaded and unloaded ZnO

All the chemicals utilized in this study were of analytical reagent (AR) grade with a purity of ≥ 98 %, procured from Sigma-Aldrich, and were used as received without any further purification. To make Solution A, 11.899 g of zinc nitrate was dissolved in 100 mL of distilled water. In Solution B, 7.564 g of oxalic acid was dissolved in 100 mL of distilled water. Solution C involved dissolving 0.1956 g of strontium nitrate in 5 mL of water. After all, three solutions had been produced, they were combined and heated to 100 °C with constant stirring for 3 h, allowing the mixture to reach boiling point. The resultant mixture was filtered, rinsed with ethanol, and dried for 5 h in a hot air oven set to 100 °C. To produce a consistent powder, the dry product was finely pounded for 30 min with a pestle and mortar. This powder was placed in a silica crucible and calcined in a muffle furnace at 460 °C for 4 h. After calcination, the furnace was allowed to cool to ambient temperature before the finished product was collected and stored for future use. This synthesis process was used to produce the sample with the optimal 3 wt% strontium loading. The same procedure was used to create samples with strontium concentrations of 1 wt%, 2 wt%, and 4 wt%. With the exception of not adding strontium nitrate, the procedure was the same for the bare ZnO sample.

2.2. Photocatalytic activity studies

The photocatalytic degradation of the azo dye Reactive Red 120 (RR 120) was studied using the Heber multi-lamp photoreactor model HML-COPACT-LP-MP88. The irradiation process was powered by four 8-watt mercury UV-A lamps with a wavelength of 365 nm. To begin the degradation process, 20 mg of the synthesised photocatalysts (ZnO and Sr-ZnO) were combined with 100 mL of a 50 ppm RR 120 dye solution at pH 7. The mixture was agitated for 30 min to reach adsorption-desorption equilibrium. The solution was then transferred to reaction tubes with inner diameters of 2.5 cm and lengths of 37 cm. To ensure uniform conditions before initiating the photodegradation process, the tubes were kept in the dark and constantly agitated. The dye solutions were exposed to UV radiation in a systematic fashion. At 10-minute intervals, 3 mL aliquots of the solution were withdrawn and centrifuged to separate the photocatalysts (REMI-R-8C). The recovered supernatant was analysed with a UV-Vis spectrophotometer to measure the photocatalysts degrading efficacy on RR 120. Parallel photodegradation experiments were also performed under direct sunlight, maintaining identical sampling and analysis intervals. UV-Vis spectroscopy was also used to determine the photocatalytic performance of these samples under natural sunlight. The efficiency of dye degradation was estimated using the formula in Eq. (1), providing a comprehensive assessment of the photocatalysts' ability to degrade the azo dye under both UV and solar irradiation conditions. This systematic approach established the efficacy of ZnO and Sr-ZnO photocatalysts in advanced environmental remediation.

$$\text{Degradation efficiency of RR120 dye } (\%) = \frac{C_0 - C_t}{C_0} \text{x} 100 \quad (1)$$

where C_0 is the RR 120 dye's initial concentration and C_t is the dye concentration after irradiation for a specific time t.

Comprehensive information regarding the materials and reagents used, the isolation of test pathogens, the characterization techniques employed, the antibacterial assay methodology, and the GC-MS analysis is provided in the supplementary section. Table S1 (see Supporting Information) displays the chemical structure of the dye, along with its respective absorption maximum.

3. Results and discussion

3.1. Crystallographic and optical features

3.1.1. Evaluation of XRD profiles

The X-ray diffraction (XRD) patterns in Fig. 1, shows the structural properties of pure ZnO (a) and Sr-loaded ZnO photocatalysts with different loading concentrations: 1 wt% (b), 2 wt% (c), 3 wt% (d), and 4 wt% (e). The samples' high crystallinity is confirmed by strong peaks at 2θ values of 31.8°, 34.4°, 36.2°, 47.5°, 56.6°, 62.9°, 66.4°, 68.0°, 69.1°, 73.0° and 77.0° which correspond to the (100), (002), (101), (102), (110), (103), (200), (112), (201), (004) and (202) planes,

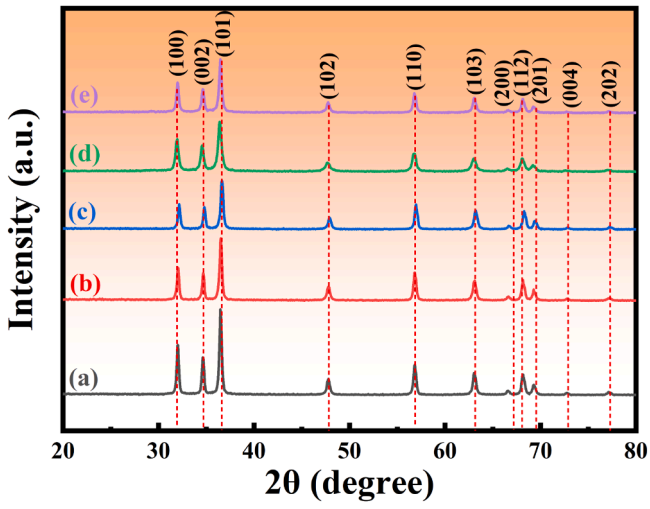

Fig. 1. X-ray diffraction (XRD) patterns of (a) pure ZnO and Sr-doped ZnO photocatalysts with varying Sr concentrations: (b) 1 wt%, (c) 2 wt%, (d) 3 wt%, and (e) 4 wt%.

respectively [30–33]. No additional impurity peaks attributable to strontium oxides or other Sr-related phases were observed when the Sr loading concentration increased from 1 wt% to 4 wt%. This suggests that Sr is successfully absorbed into the ZnO lattice without generating distinct phases, implying substitutional loading. However, modest fluctuations in peak intensity and broadening are visible as Sr content increases, which could be related to lattice tension, flaws, or a reduction in crystallite size caused by Sr integration. Such structural alterations may have an impact on Sr-loaded ZnO's electrical characteristics and, as a result, photocatalytic activity. Overall, the XRD examination verifies the effective synthesis of Sr-loaded ZnO photocatalysts with intact wurtzite structure. Slight variations in peak intensity and broadening suggest that Sr inclusion may have an effect on crystallite size and lattice strain. These structural changes are projected to significantly improve Sr-ZnO's photocatalytic performance, making it a potential material for environmental remediation applications such as wastewater treatment and pollutant degradation under light irradiation [34].

3.1.2. FT-IR profile interpretation

Fig. S1 (see Supporting information) presents the FT-IR spectra of pure ZnO and Sr-doped ZnO photocatalysts with varying Sr concentrations. A broad absorption band observed in the range of 3200–3600 cm^{-1} corresponds to O–H stretching vibrations, indicative of surface hydroxyl groups. These groups are known to facilitate improved photocatalytic activity by promoting effective charge carrier separation. The presence of a distinct band between 1600 and 1660 cm^{-1} is attributed bending vibration of hydroxyl (-OH), likely due to surface adsorbed water. In the lower wavenumber region (400–600 cm^{-1}), characteristic Zn–O stretching vibrations confirm the formation of ZnO nanoparticles. Across all Sr loadings, the FT-IR spectra exhibit nearly identical vibrational profiles, with no emergence of additional peaks. However, slight variations in peak intensities and minor shifts in band positions suggest subtle modifications in surface chemical environments and bonding configurations due to Sr incorporation. These spectral changes imply potential influences on the photocatalytic behavior of the materials, although the core ZnO structure remains largely preserved [35,36].

3.1.3. Vibrational mode identification by FT-Raman spectroscopy

Fig. 2 shows the FT-Raman spectra of pure ZnO and Sr-doped ZnO photocatalysts at different Sr concentrations (1 wt%, 2 wt%, 3 wt%, and 4 wt%). The detected vibrational characteristics represent major structural alterations and defect states caused by Sr inclusion [37,38]. The phonon vibrations of the wurtzite ZnO lattice are responsible for the characteristic Raman modes E_{2L} (in the low-frequency region, approximately 265 cm^{-1}), E_{2H}-E_{2L} mode (437 cm^{-1}), and E_{2H} (in the high-frequency region, 757 cm^{-1}). These modes are highly defined in the undoped ZnO sample, indicating its intrinsic crystalline structure. Raman spectra show significant changes after Sr doping, including increased peak intensities and modest peak shifts, especially in the E_{2H} area. These spectrum shifts confirm that Sr ions were successfully substituted into the ZnO lattice, resulting in local structural distortions and increased crystallinity. The gradual increase in Raman mode strength with increasing Sr concentration indicates improved phonon coupling and lattice ordering. Such enhancements are expected to greatly increase the photocatalytic performance of Sr-doped ZnO nanostructures by fostering more efficient charge carrier dynamics and decreasing recombination rates.

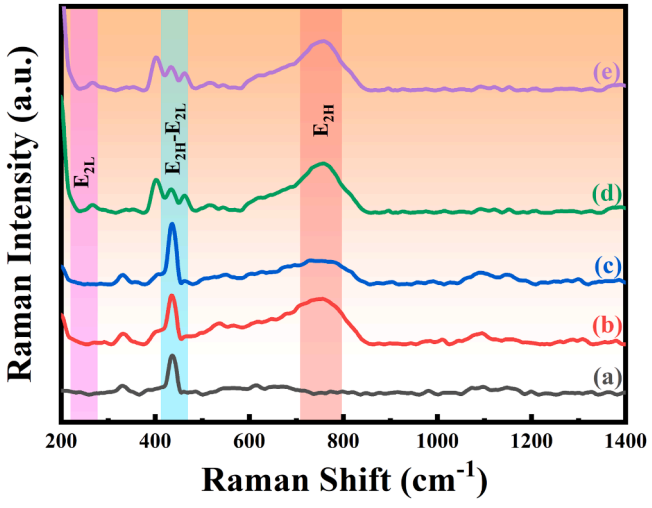

Fig. 2. FT-Raman spectra of (a) ZnO and Sr-doped ZnO photocatalysts at varying Sr concentrations: (b) 1 wt%, (c) 2 wt%, (d) 3 wt%, and (e) 4 wt%.

3.1.4. PL-based investigation of electron–hole dynamics

Fig. S2 depicts the photoluminescence (PL) spectra of pure ZnO and Sr-doped ZnO photocatalysts with varying strontium loading levels (1, 2, 3, and 4 wt%). PL spectroscopy is a useful technique for investigating the recombination behaviour of photogenerated charge carriers in semiconductor materials. The undoped ZnO sample has a robust and broad emission band in the 400–550 nm wavelength range, encompassing both near-band-edge (NBE) and deep-level emissions (DLE). The NBE emission is usually related to the recombination of free excitons along the conduction and valence bands, whereas the DLE corresponds to intrinsic defects such as oxygen vacancies, zinc interstitials, and surface states within the ZnO lattice [39–41]. The introduction of Sr into the ZnO matrix results in a considerable drop in PL intensity across the spectrum. The suppression of PL emission reflects a slower recombination rate of photogenerated electron-hole pairs. The drop-in intensity means that Sr doping introduces localised states or affects the defect landscape in such a way that charge carriers can be separated and transferred more efficiently rather than recombining radiatively. Compared to bare ZnO, the doped samples exhibit the lowest PL intensity, indicating that they have the most effective charge carrier separation and the fewest recombination losses, which is extremely useful for increasing photocatalytic efficiency. These findings show that Sr doping not only modifies the electrical structure of ZnO but also improves its optical and charge transport capabilities. The reduction in radiative recombination caused by PL quenching is a clear indication of increased photocatalytic capability. As a result, regulated Sr inclusion appears to be a promising technique for improving ZnO-based photocatalysts for environmental and energy applications.

3.1.5. UV-DRS analysis

Fig. S3 shows the UV-Vis diffuse reflectance spectra (DRS) and Kubelka-Munk (KM) plots for ZnO and strontium-loaded ZnO (Sr-ZnO) photocatalysts with loading concentrations of 1–4 wt%, respectively. The UV-Vis reflectance spectra (Fig. S3a) show the light absorption characteristics of both unloaded and Sr-ZnO samples, providing important information on their optical properties. The Kubelka-Munk function, F(R), is used to calculate optical band gaps using conventional equations [42].

$$(F(R)h\upsilon)^n = A\,(h\upsilon - E_g) \tag{2}$$

$$F(R) = \frac{(1-R)^2}{2R} \tag{3}$$

In these equations, R denotes the diffuse reflectance of the material, and hv represents the photon energy, where h is Planck's constant and ν is the photon frequency. The band gap of pure ZnO was determined to be 3.19 eV (Fig. S3b), consistent with previously reported values in the literature. Upon Sr doping, significant changes in the band gap were observed. At 1 wt% Sr-ZnO, the band gap slightly decreases to 3.18 eV (Fig. S3c), which may be attributed to quantum confinement effects or lattice distortion induced by the incorporation of Sr ions. As the Sr concentration increases, the band gap gradually decreases, measuring

3.17 eV for 2 wt%, 3.16 eV for 3 wt%, and then slightly rises again to 3.18 eV for 4 wt% Sr-ZnO (Fig. S3d-**f**). The observed fluctuations in band gap energy with varying Sr content are critical for tuning the optical and photocatalytic properties of ZnO. A decreased band gap favours enhanced absorption of light, which can improve photocatalytic activity, whereas a reduced band gap shifts the absorption edge toward the visible spectrum, making the material more suitable for solar-driven applications. These results indicate that precise control over Sr doping concentration can optimize ZnO's performance in various fields such as optoelectronics, photovoltaics, and environmental remediation, particularly for photocatalytic degradation of pollutants [43].

3.2. Morphological studies

3.2.1. FE-SEM analysis

Fig. 3 shows field emission scanning electron microscopy (FE-SEM) images of (a-c) pure ZnO and (d-f) 3 wt% Sr-loaded ZnO (Sr-ZnO) photocatalysts at different magnifications and locations. These micrographs provide valuable information regarding the surface shape and particle distribution of the synthesised nanomaterials. Pure ZnO nanoparticles (Fig. 3a-c) have an aggregated structure made up of uniformly dispersed, almost spherical grains [33,34]. The particles are firmly packed with moderate porosity, as is characteristic of ZnO synthesised using wet chemical or hydrothermal methods. The ZnO particles are nanometres in size, with well-defined grain boundaries and a relatively smooth surface texture, confirming their crystalline structure. The nanoparticles in the Sr-ZnO sample (Fig. 3d-f) have better dispersion and appear slightly smaller and more uniform than the unloaded ZnO, as seen by the measured particle sizes displayed in the annotated photos. Incorporating Sr^{2+} ions into the ZnO lattice may cause lattice deformation and limit excessive grain development, leading to finer particles. Furthermore, the surface of Sr-ZnO appears rougher and less compact than pure ZnO, indicating potential photocatalytic activity due to the exposure of additional active sites. The morphological differences between pure ZnO and Sr-loaded ZnO show that Sr was successfully incorporated into the ZnO matrix. This loading has an impact not only on the photocatalyst's structural properties but also on its optical and electrical behaviour. Sr-ZnO's reduced particle size and increased surface roughness could allow for greater light absorption and better interaction with pollutants in photocatalytic applications, making it a promising candidate for environmental remediation processes, particularly wastewater treatment [44,45].

3.2.2. HR-TEM analysis

Fig. 4 presents a comprehensive exploration of the morphological and structural characteristics of the 3 wt% Sr-doped ZnO (Sr–ZnO) photocatalyst using transmission electron microscopy (TEM) and high-resolution TEM (HR-TEM) techniques. The low- and intermediate-magnification TEM images (Fig. 4a–c), obtained from different regions of the sample, reveal a diverse particle morphology consisting of both hexagonal and quasi-spherical nanoparticles. This morphological heterogeneity implies a non-uniform nucleation and growth process, likely modulated by the incorporation of Sr during synthesis. HR-TEM micrographs (Figs. 4d and 4e) further disclose well-defined and periodic lattice fringes, reflecting the high degree of crystallinity within the Sr–ZnO structure. These lattice patterns correspond to characteristic planes of ZnO, confirming that Sr doping does not significantly disturb the parent ZnO lattice structure. To gain further insight into the lattice orientation and order, fast Fourier transform (FFT) patterns were extracted from specific areas marked in Fig. 4e (yellow square and red circle), and are depicted in Fig. 4f and 4j. The symmetrical and periodic diffraction spots in the FFT images validate the presence of well-ordered crystalline domains. The frequency-specific features identified in the FFT patterns were selectively enhanced using mask filtering, and the resulting filtered images are shown in Fig. 4g and 4k. These were subsequently processed through inverse fast Fourier transform (IFFT) to reconstruct real-space lattice information with reduced background noise, as illustrated in Figs. 4i and 4m. The IFFT-enhanced images significantly improve the clarity of lattice fringes, enabling precise estimation of interplanar distances and orientation. Furthermore, the

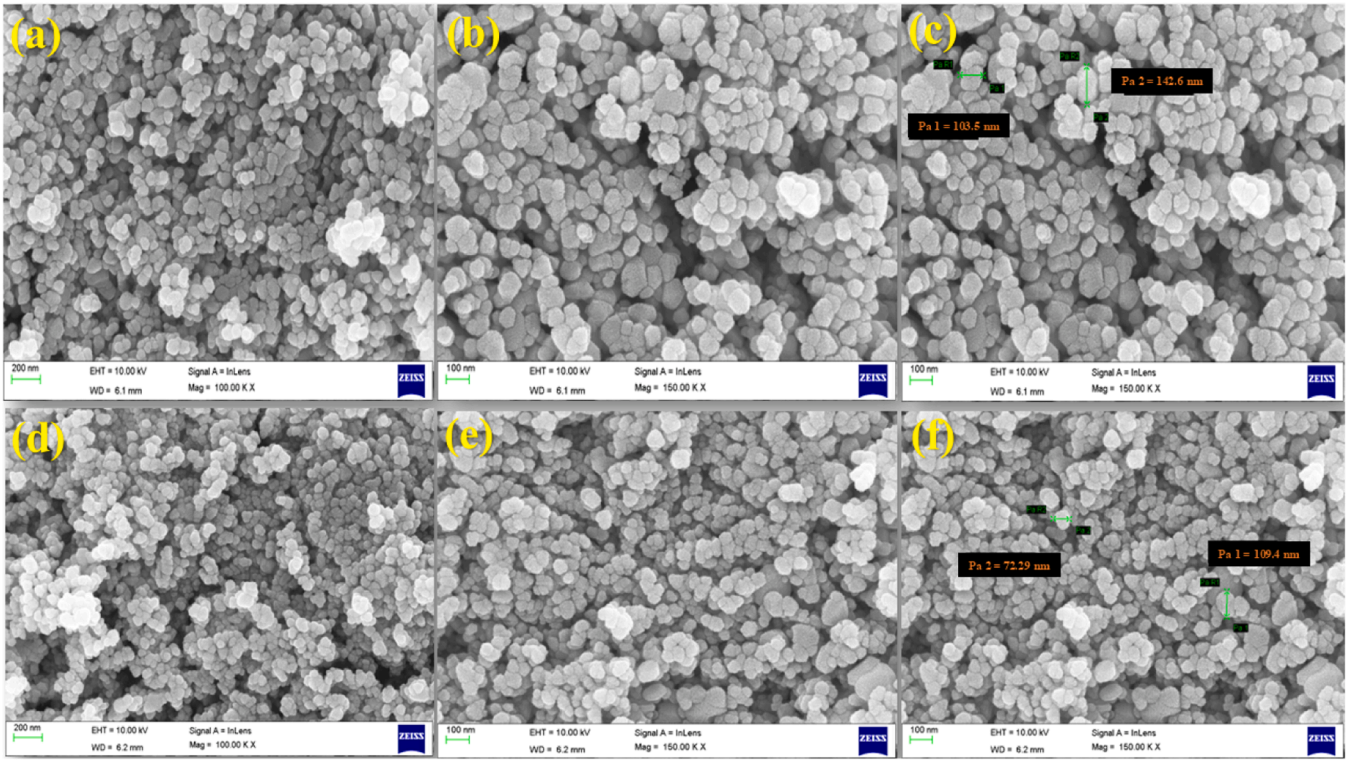

Fig. 3. FE-SEM images of (a-c) ZnO and (d-f) 3 wt% Sr-ZnO photocatalysts.

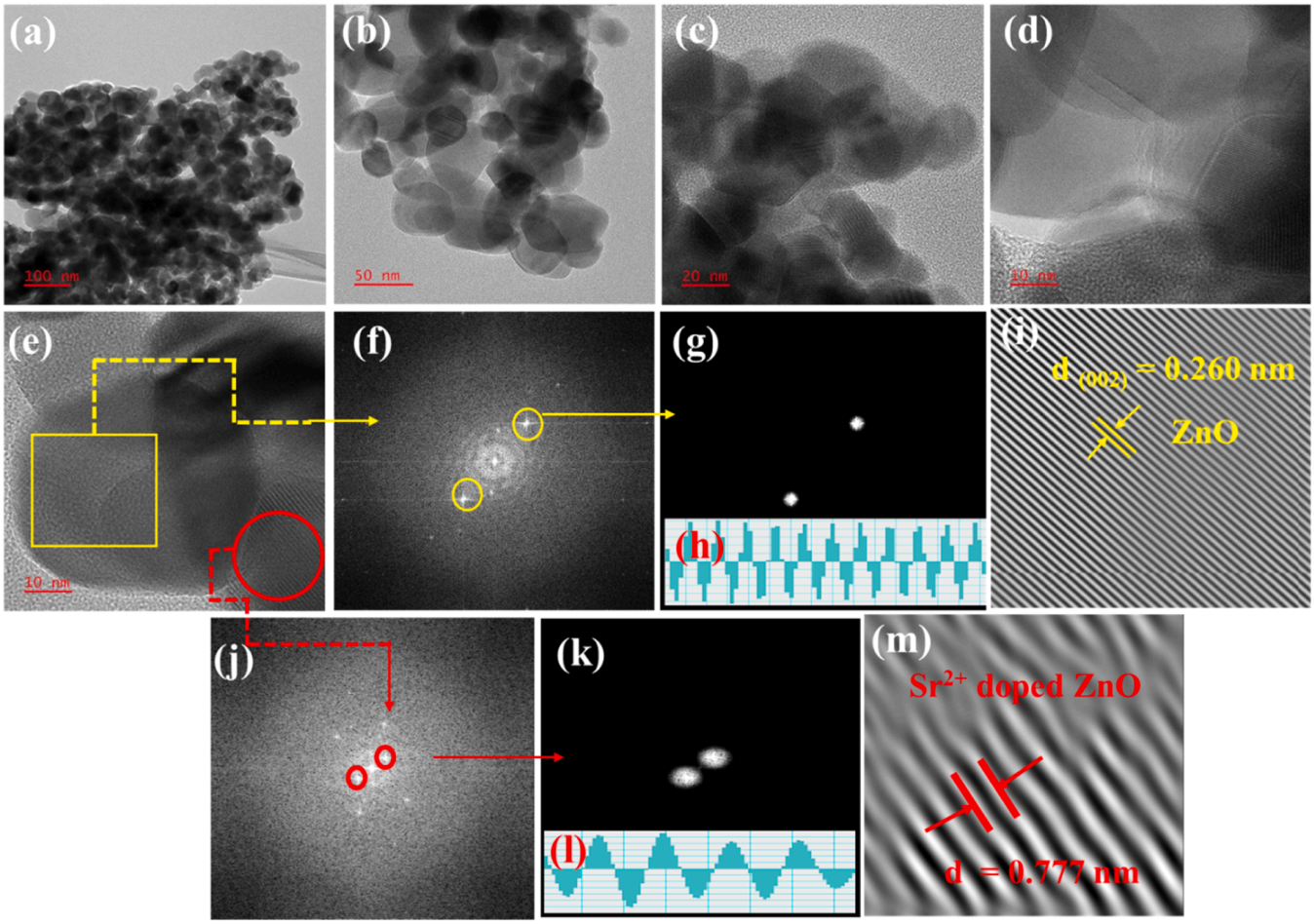

Fig. 4. (a-c) TEM images, (d and e) HR-TEM images of 3 wt% Sr-ZnO photocatalyst, (f and j) corresponding FFT, (g and k) mask area, (h and l) profile of IFFT, (i and m) IFFT images with crystalline planes of Sr-ZnO.

intensity line profiles (Fig. 4h and 4l), derived from the IFFT regions, provide quantitative evidence of consistent fringe spacing and periodicity, thus supporting the effective integration of Sr^{2+} ions into the ZnO matrix without disrupting the overall crystallographic integrity.

HR-TEM analysis of Sr-doped ZnO revealed two distinct interplanar spacings of approximately 0.260 nm and 0.777 nm, offering insight into the structural modifications induced by Sr incorporation. The d-spacing of 0.260 nm corresponds well to the (002) plane of the wurtzite ZnO structure, confirming that the host lattice remains largely intact. In the HR-TEM analysis of Sr-doped ZnO, the observation of a lattice fringe with a d-spacing of 0.777 nm is intriguing, particularly since no corresponding peak is detected in the X-ray diffraction (XRD) pattern. The absence of a matching XRD peak suggests that this feature does not arise from a well-crystallized, long-range ordered secondary phase such as SrO or $Sr(OH)_2$, which would otherwise manifest distinct reflections in the XRD spectrum. Instead, the 0.777 nm spacing is more plausibly attributed to local structural distortions, interfacial lattice mismatch regions, or defect-rich domains induced by Sr incorporation. The ionic radius of Sr^{2+} (1.18 Å) is significantly larger than that of Zn^{2+} (0.74 Å), and its substitution or interstitial presence within the ZnO lattice can induce localized strain, lattice expansion, or the formation of planar defects or stacking faults, particularly near grain boundaries. Such structural features are often non-periodic or poorly ordered, lacking sufficient crystallinity to produce detectable XRD peaks but clearly observable in high-resolution TEM due to its sensitivity to local atomic arrangements. Furthermore, in some cases, Sr segregation at the nanoscale, especially at surface or interface regions, can result in amorphous or partially ordered domains, which again evade detection by XRD but manifest as distinct lattice spacings in HR-TEM. Therefore, the 0.777 nm d-spacing likely reflects a short-range ordered region or strain-induced lattice expansion due to Sr doping, rather than a separate crystalline phase.

3.2.3. *EDS and elemental mapping analysis*

The catalysts were tested using energy dispersive spectroscopy, elemental mapping, and SEM. The elemental composition of ZnO and Sr-ZnO catalysts was established using EDS analysis. Fig. S4 depicts the elemental composition of the catalysts and the elements present in a specific area, as shown in Tables S2 and S3 (see Supporting material). The elemental composition of Sr-ZnO catalysts indicates effective Sr loading over ZnO. The elements O and Zn were largely obtained in naked EDS at 0.2–0.6 and 0.8–1.2 keV, respectively (Fig. S4a). However, a new peak between 1.8 and 2.0 KeV emerged, indicating the presence of Sr over ZnO, as seen in Fig. S4b [46,47]. Fig. S5 illustrates the elemental mapping of the constituent elements in both pure ZnO and Sr-doped ZnO photocatalysts.

3.2.4. *XPS analysis*

Fig. 5. shows the X-ray photoelectron spectroscopy (XPS) examination of Sr-ZnO photocatalysts, which provides important information about their elemental composition, oxidation states, and chemical bonding. Fig. 5a shows the survey spectrum, which confirms the presence of Zn, O, and Sr in the Sr-ZnO sample. The peaks corresponding to Zn 2p, O 1 s, and Sr 3d demonstrate the successful incorporation of Sr into the ZnO lattice, supporting the structural alteration caused by loading. Fig. 5b depicts the high-resolution Zn 2p spectrum, which

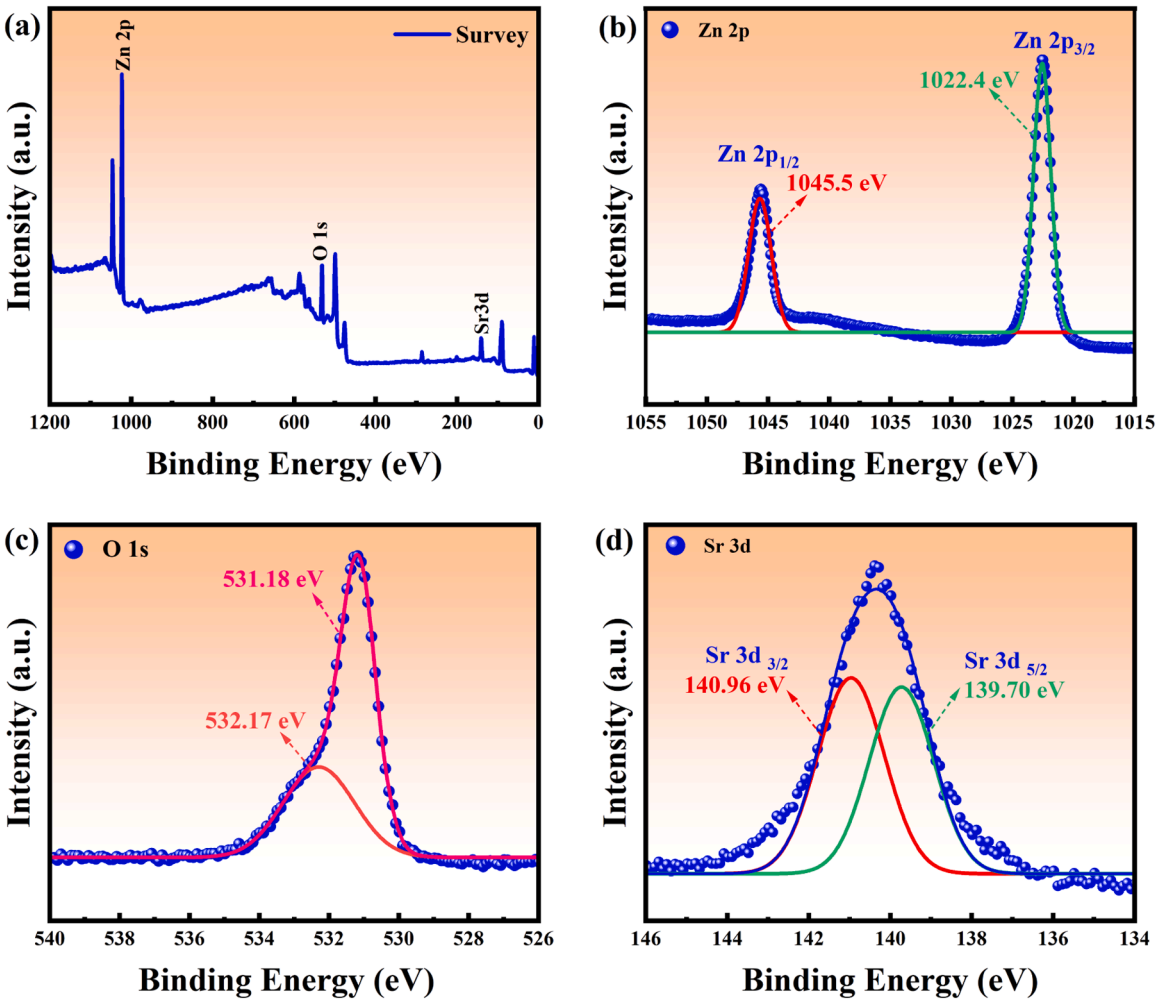

Fig. 5. XPS of Sr-ZnO photocatalysts, (a) survey spectrum, (b) Zn 2p, (c) O 1 s and (d) Sr 3d.

contains two distinct peaks at 1022.4 eV and 1045.5 eV, which correspond to Zn $2p_{3/2}$ and Zn $2p_{1/2}$, respectively. These binding energies align with Zn^{2+} in ZnO, indicating that Zn remains in its anticipated oxidation state without metallic Zn or other oxidation states. The peak positions indicate negligible alterations due to Sr loading, implying that Sr inclusion has no substantial effect on the Zn 2p electronic structure but may contribute to defect generation.

Fig. 5**c** depicts the O 1 s spectrum, which shows two different peaks at 531.18 eV and 532.17 eV. The peak at 531.18 eV corresponds to lattice oxygen, verifying ZnO's structural integrity. The peak at 532.17 eV is due to oxygen vacancies and chemisorbed oxygen species, which play an important role in improving photocatalytic performance by trapping charge carriers and boosting surface reactions. The existence of oxygen vacancies shows that Sr loading alters the defect states in ZnO, perhaps improving charge separation and overall photocatalytic activity. Fig. 5d depicts the Sr 3d spectrum, indicating the incorporation of Sr into the ZnO matrix. The Sr 3d spectrum shows two peaks at 139.70 eV and 140.96 eV, which correspond to Sr $3d_{5/2}$ and Sr $3d_{3/2}$, respectively. These peaks confirm the successful loading of Sr^{2+} in the ZnO lattice. The insertion of Sr most likely causes lattice distortions and defect development, which can improve the material's electrical characteristics and photocatalytic performance. Overall, the XPS results demonstrate the effective synthesis of Sr-loaded ZnO with well-defined oxidation states and defect architectures. The presence of oxygen vacancies and Sr incorporation are critical for altering the electronic structure, minimising charge carrier recombination, and increasing photocatalytic activity. These results are consistent with previous characterisation approaches, supporting the importance of Sr loading in modifying the physicochemical parameters of ZnO for environmental applications, particularly photocatalytic water treatment [48].

4. Photocatalytic activity study

4.1. Photodegradation of RR 120 under UV-A light

The Fig. 6 shows the UV-Vis absorption spectra of RR 120 dye (50 ppm, pH 7) exposed to UV-A light in the presence of Sr-loaded ZnO photocatalysts with varying Sr concentrations (1 wt%, 2 wt%, 3 wt%, and 4 wt%) throughout a variety of irradiation times (0–70 min). The absorption peak of RR 120, located at around 523 nm, rapidly decreases with increasing irradiation time, indicating that the dye is successfully photodegraded. The absorbance of clean ZnO (Fig. 6a) steadily decreases, indicating photocatalytic activity. However, adding Sr to ZnO improves photocatalytic performance. Among the loaded samples, 3 wt % Sr-ZnO (Fig. 6b) exhibits a faster rate of dye degradation than pure ZnO, implying that Sr loading promotes charge separation. The best degradation efficiency is obtained with 3 wt% Sr-ZnO (Fig. 6d), where the dye absorption peak drops dramatically in a shorter time period. This shows that 3 wt% Sr loading maximises charge carrier separation, hence boosting photocatalytic efficiency. However, at 4 wt% Sr-ZnO (Fig. 6e), the deterioration rate slows compared to the 3 wt% sample. This decrease in efficiency could be attributable to high Sr loading, which can operate as recombination centres, preventing charge separation and lowering photocatalytic efficacy. Overall, the study shows

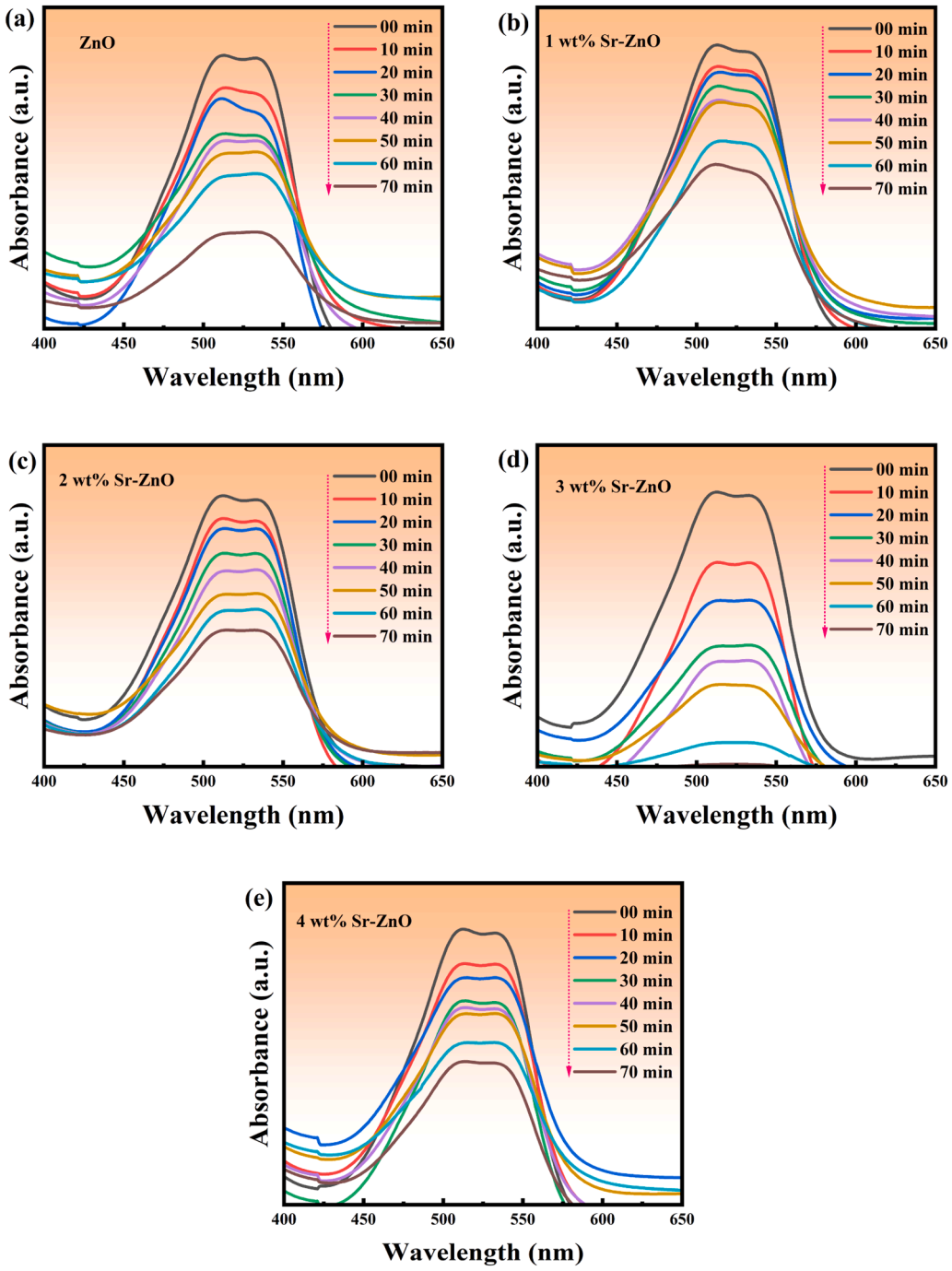

Fig. 6. UV-Vis absorption spectra of RR 120 with different irradiation time under UV-A light with (a) ZnO (b) 1 wt% (c) 2 wt% (d) 3 wt% (e) 4 wt% Sr-ZnO photocatalysts [Catalyst dosage = 20 mg; pH = 7; Dye concentration = 50 ppm].

that Sr loading has a favourable effect on ZnO, with a 3 wt% loading concentration resulting in maximum photocatalytic degradation of RR 120 dye. This shows that Sr-modified ZnO photocatalysts may be a potential material for efficient wastewater treatment under UV-A radiation.

Fig. 7 depicts the photocatalytic activity of Sr-loaded ZnO with various Sr concentrations (1–4 wt%) compared to pure ZnO under sunlight irradiation. Fig. 7a depicts the percentage of dye degradation over time, with 3 wt% Sr-ZnO having the highest degradation rate, outperforming pure ZnO and the other loaded samples. Fig. 7b shows the normalised dye concentration (C_t/C_0), which falls faster for 3 wt% Sr-ZnO, showing greater photocatalytic efficiency. Fig. 7c displays the kinetic linear fitting results, which show that dye degradation occurs in a pseudo-first-order reaction model. The calculated rate constants (k) for photocatalytic activity varied according to doping concentration. The rate constant for bare ZnO is 0.01206 min^{-1} , for Sr loadings of 1 wt% is 0.00706 min^{-1} , 2 wt% is 0.0095 min^{-1} , 3 wt% is 0.03827 min^{-1} , and 4 wt% is 0.00838 min^{-1} . The corresponding R^2 values were 0.86566 for bare ZnO, 0.89641 for 1 wt%, 0.98366 for 2 wt%, 0.90251 for 3 w%, and 0.96477 for 4 wt% Sr-ZnO. Finally, Fig. 7d compares the degradation efficiency at 70 min, revealing that 3 wt% Sr-ZnO exhibits nearly complete degradation (≈100 %), whereas pure ZnO and other loaded samples exhibit lower efficiency. Overall, the findings demonstrate that Sr loading greatly increases ZnO's photocatalytic activity, with 3 wt%

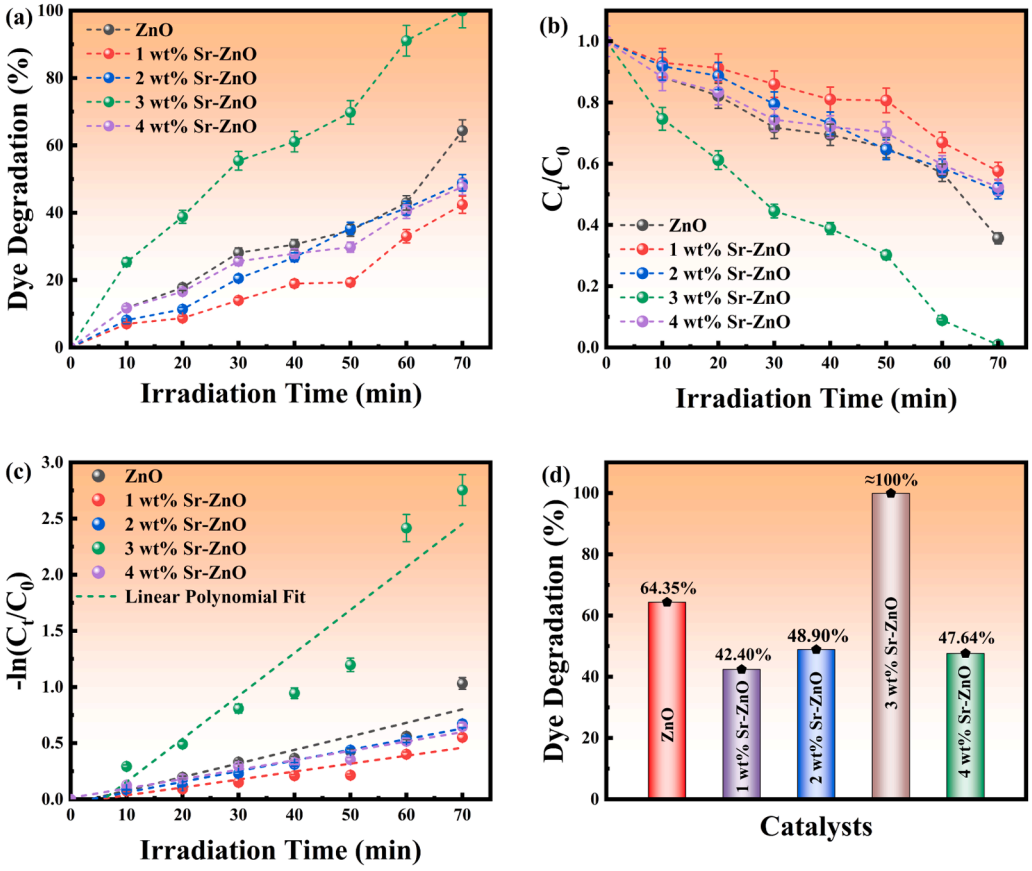

Fig. 7. (a) Photocatalytic activity results, (b) Normalized absorbance spectra (C_t/C_0), (c) Kinetic linear fitting results (d) Comparison of photocatalytic activity at 70 min with, 1 wt%, 2 wt%, 3 wt% and 4 wt% Sr-ZnO photocatalysts.

Sr-ZnO being the most effective composition for dye degradation. This improvement is likely due to enhanced charge separation, decreased recombination, and greater light absorption, making it an attractive candidate for wastewater treatment applications.

4.1.1. Photodegradation of RR 120 under sunlight

Fig. 8 depicts the UV-Vis absorption spectra of an RR 120 dye solution at various irradiation durations under sunlight using (a) pure ZnO and (b) 3 wt% Sr-ZnO as photocatalysts. The absorbance peak at 523 nm is the distinctive absorption of RR 120 dye. As the irradiation period increases (from 0 to 50 min), the absorbance intensity drops, indicating dye degradation. In Fig. 8a, ZnO has a steady decrease in absorbance, indicating modest photocatalytic activity. However, in Figs. 8b, 3 wt% Sr-ZnO shows a more dramatic decrease in absorbance, indicating improved photocatalytic activity. Sr-loaded ZnO exhibits higher activity due to improved charge separation, reduced electron-hole recombination, and increased light absorption. The photocatalytic degradation happens when electron-hole pairs are generated by sunlight exposure, resulting in the creation of reactive oxygen species (ROS) that break down the dye molecules. The more effective degradation observed with 3 wt% Sr-ZnO shows that Sr loading increases ZnO's photocatalytic efficiency. Overall, the results reveal that Sr loading greatly increases

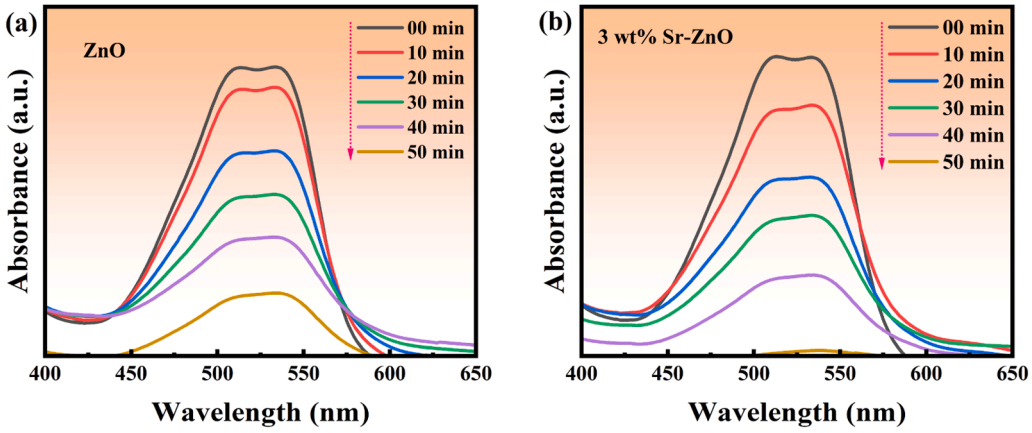

Fig. 8. UV-Vis absorption spectra of RR 120 with different irradiation time under Sunlight irradiation with (a) ZnO (b) 3 wt% photocatalysts [Catalyst dosage = 20 mg; pH = 7; Dye concentration = 50 ppm].

ZnO's photocatalytic ability, with 3 wt% Sr-ZnO demonstrating greater degradation efficiency. This makes it an attractive material for environmental remediation, particularly in wastewater treatment applications.

Fig. 9 shows the photocatalytic performance of ZnO and 3 wt% Sr-ZnO for RR 120 dye degradation when exposed to sunshine. Fig. 9a shows the percentage of dye degradation over time, demonstrating that 3 wt% Sr-ZnO has much higher degradation efficiency than pure ZnO. This suggests that Sr loading boosts ZnO's photocatalytic activity. Fig. 9b plots the normalised dye concentration (C_t/C_0) vs irradiation time. The concentration of RR 120 dye falls more quickly with 3 wt% Sr-ZnO, showing higher degradation efficiency over ZnO. This demonstrates that Sr loading enhances charge carrier separation, lowering recombination losses and accelerating dye degradation. Linear fitting of degradation. The kinetics revealed rate constants (k) of 0.02961 min^{-1} for bare ZnO and 0.0475 min^{-1} for 3 wt% Sr-ZnO. The R^2 values for bare ZnO is 0.92552, and 3 wt% Sr-ZnO is 0.90571, as seen in Fig. 9c. Finally, Fig. 9d compares the degrading efficiency of ZnO and 3 wt% Sr-ZnO after 50 min. The dye degradation efficiency of ZnO is 78.4 wt%, whereas 3 wt% Sr-ZnO reaches ≈ 100 % degradation, demonstrating its superior performance. Overall, these findings show that Sr loading greatly increases the photocatalytic effectiveness of ZnO, making 3 wt% Sr-ZnO a potential material for environmental applications such as wastewater treatment.

4.2. *Effect of catalyst loading and initial pH*

The performance of 3 wt% Sr-loaded ZnO (Sr-ZnO) nanoparticles in photocatalytic degradation was thoroughly evaluated at various pH levels and catalyst dosages. The purpose of this investigation was to identify the optimal conditions for efficiently eliminating RR 120 dye under UV light exposure, and the results are shown in Fig. 10 As demonstrated in Fig. 10a, the solution pH had a substantial effect on degradation performance. Using 20 mg of Sr-ZnO and 70 min of UV-A irradiation, the degradation efficiency increased with increasing pH, reaching a high of around ≈ 100 % at pH 7. At acidic pH levels (pH 3 and 5), breakdown efficiency was lower, at 58 % and 72 %, respectively. Excess H^+ ions and dye molecules compete for active sites, resulting in reduced production of hydroxyl radicals ($^{\bullet}OH$). Under neutral conditions, optimal charge interaction between the dye and the catalyst surface led to increased adsorption and reactive species formation. At higher pH levels (9 and 11), degradation somewhat decreased to 96 % and 88 %, probably due to electrostatic repulsion between negatively charged catalyst surfaces and dye molecules. Fig. 10b shows how the catalyst dose affects the photocatalytic degradation efficiency of RR 120 dye after 30 min of UV-A light exposure at pH 7. The 3 wt% Sr-ZnO catalyst was tested at dosages of 10 mg, 30 mg, 50 mg, and 70 mg. At lower catalyst concentrations of 10 mg and 30 mg, degradation efficiencies were relatively low, at 19.9 % and 37.6 %. This poor performance can be due to a scarcity of active sites accessible for photocatalytic processes. However, when the dosage was increased to 50 mg, the degradation efficiency increased dramatically to around ≈ 100 %, demonstrating the optimal amount of catalyst for maximum light absorption and interaction with dye molecules. However, increasing the dose to 70 mg resulted in a 96.5 % drop in degradation efficiency. This drop is most likely caused by abundant catalyst particles, which cause light scattering, limited light penetration, and probable agglomeration, all of which impede the photocatalytic process. In conclusion, neutral pH 7 and a catalyst dosage of 50 mg was discovered to be best for maximal photocatalytic degradation, providing useful insight into process optimisation for wastewater treatment applications.

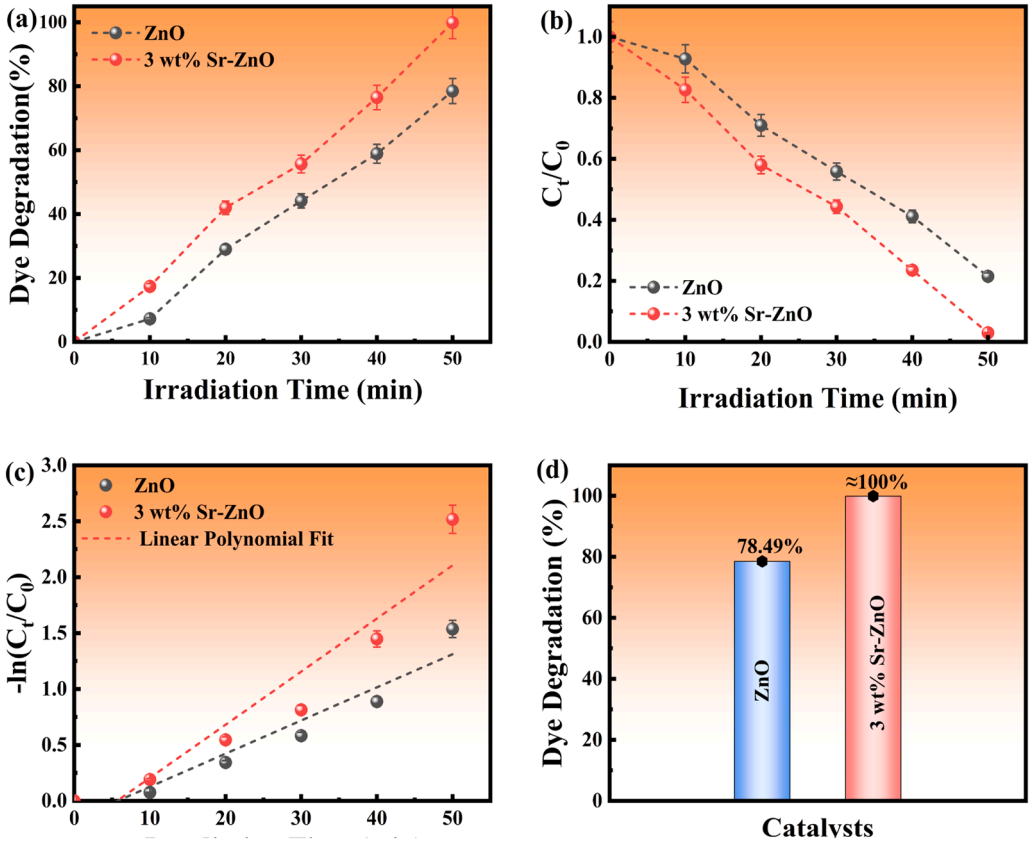

Fig. 9. (a) Photocatalytic activity results, (b) Normalized absorbance spectra (C_t/C_0), (c) Kinetic linear fitting results (d) Comparison of photocatalytic activity at 50 min with ZnO, 3 wt% Sr-ZnO photocatalysts.

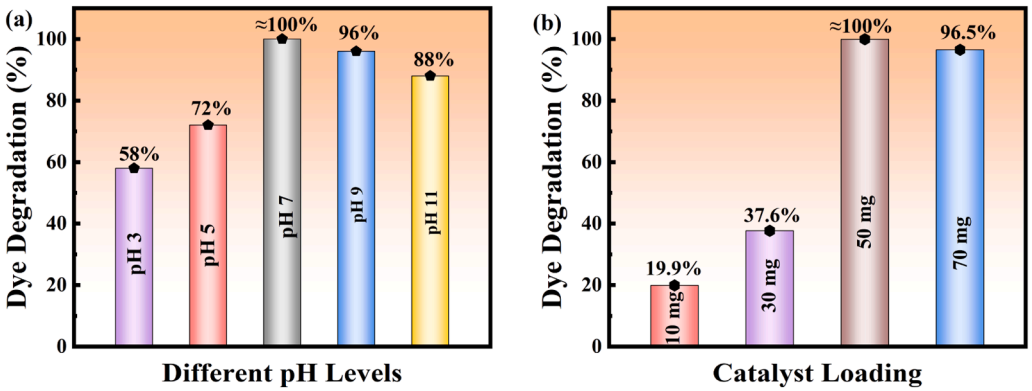

Fig. 10. (a) The effect of pH levels (using 20 mg of 3 wt% Sr-ZnO; 70-minute irradiation time). (b) Effects of catalyst dosage on photocatalytic degradation of RR 120 after 30 min of UV-A light at pH 7.

4.3. Reusability and trapping

To determine the practical applicability of 3 wt% Sr-loaded ZnO, the reusability and active species involved in the photocatalytic degradation of RR 120 dye under UV-A light were examined. These tests are necessary to establish the catalyst's stability across numerous cycles and to comprehend the underlying degradation mechanism in Fig. 11. Fig. 11a shows the reusability performance of 3 wt% Sr-ZnO across four consecutive cycles for the degradation of RR 120 dye under UV-A irradiation (30 min, pH 7, 50 mg catalyst dosage). The degrading efficiency remained high throughout, with ≈100 % in the first cycle, gradually dropping to 97 %, 95 %, and 91 wt% in the second, third, and fourth cycles, respectively. This steady drop can be attributed to slight catalyst deactivation caused by surface fouling, partial loss of active sites, or intermediate adsorption during each cycle. Despite this, the photocatalyst retained over 90 % efficiency after several uses, indicating outstanding recyclability and structural integrity during repeated operation. Fig. 11b depicts the impact of different scavengers on the photocatalytic degradation efficiency of RR 120 dye under UV. A light irradiation for 50 min at neutral pH (pH 7) with 50 mg of catalyst. The judicious employment of certain scavengers allows for the detection of key reactive species involved in the degradation mechanism. Benzoquinone (BQ), a selective quencher of superoxide radicals ($O_2^{\bullet-}$), significantly suppressed photocatalytic activity, reducing degradation efficiency by approximately 25 %. This significant drop underlines the importance of superoxide radicals as the major reactive species. Using potassium iodide (KI) to scavenge photogenerated holes (h^+) lowered degradation efficiency to 48 %, indicating a significant contribution from holes to the process. *Tert*-butanol (TBA), a well-known hydroxyl radical ($^{\bullet}OH$) scavenger, resulted in a 49.5 % degradation efficiency, showing a moderate but significant function for hydroxyl radicals. Furthermore, silver nitrate ($AgNO_3$), an electron (e^-) scavenger, resulted in 63 % degradation, indicating a minor but significant participation of electrons in the chemical pathway. The control experiment, which did not include a scavenger, resulted in nearly total destruction (≈100 %), demonstrating the synergistic action of several reactive oxygen species. These findings show that the photocatalytic degradation of RR 120 using Sr-ZnO is primarily controlled by the formation of superoxide radicals, with significant contributions from hydroxyl radicals and photogenerated holes, indicating a multi-pathway degradation mechanism.

4.4. Degradation pathway of RR 120 using GC-MS

The photocatalytic degradation of Reactive Red 120 (RR 120) under UV-A light using 3 wt% strontium-doped ZnO (Sr-ZnO) was thoroughly investigated through gas chromatography–mass spectrometry (GC-MS). This high-resolution analytical method facilitated the identification of numerous intermediate products, detailed in Table S4. Based on the observed molecular ion peaks and fragmentation patterns, a plausible degradation mechanism has been mapped out and depicted in Fig. 12. It is important to recognize that during photodegradation, the parent dye does not immediately break down into harmless substances; instead, it often forms transitional compounds, some of which may retain toxicity or environmental persistence.

In this study, three major intermediates labeled **IIP 1**, **IIP 2**, and **IIP 3** were isolated as significant products formed during the UV-A-assisted degradation of RR 120 under neutral pH conditions in the presence of Sr-ZnO. The degradation pathway was initiated by the rupture of the azo linkage (–N=N–) within RR 120, yielding two primary intermediates: **IIP 1**, structurally identified as a triazine-linked aminonaphthalene

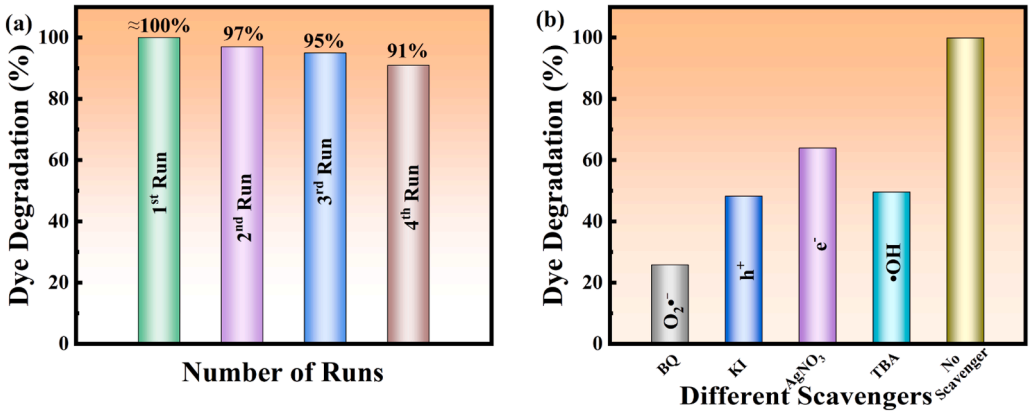

Fig. 11. (a) Reusability results (b) Effect of scavengers in pH 7 with catalyst dosage of 50 mg in RR 120 degradation under UV-A light with 30 min of irradiation.

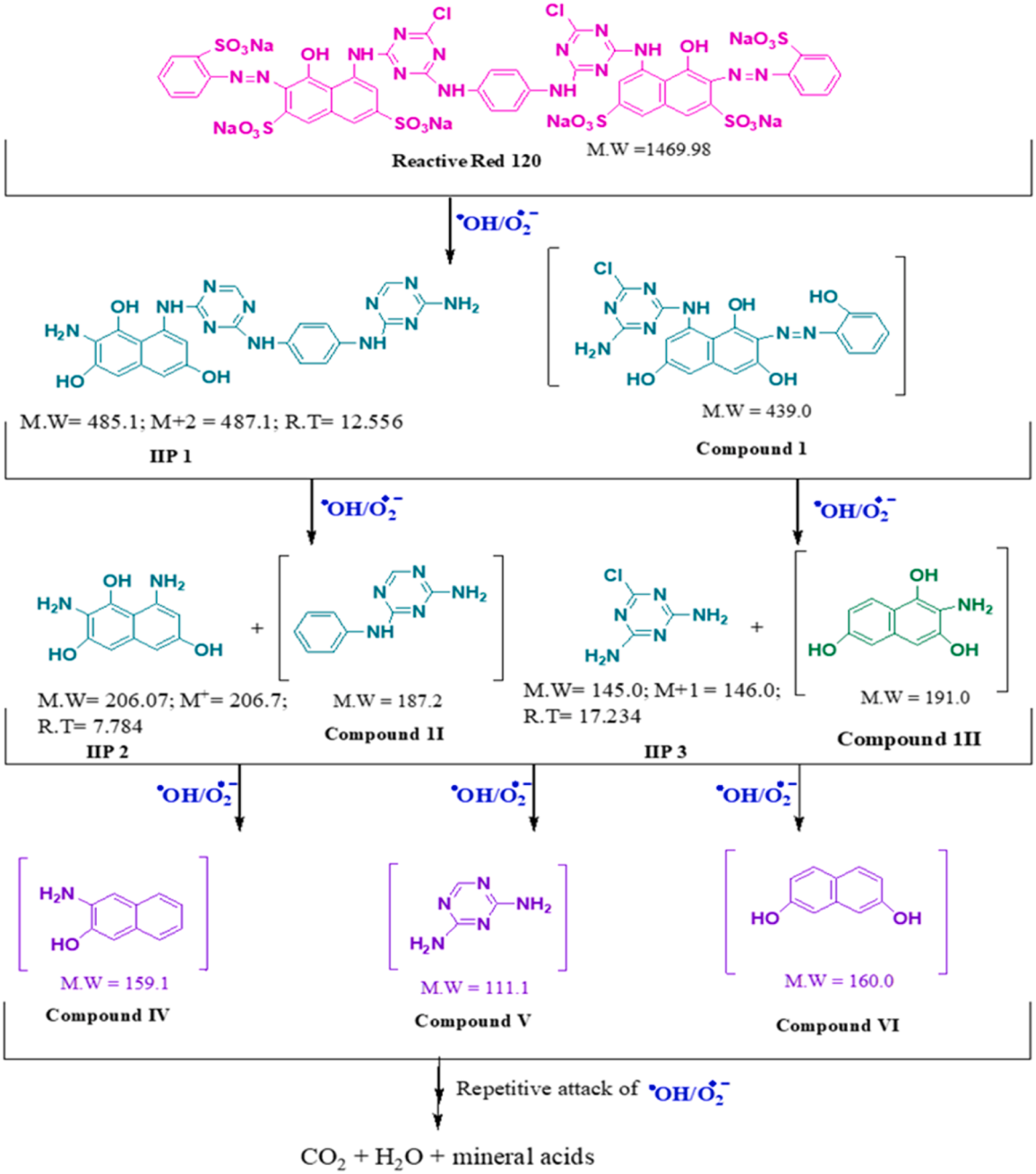

Fig. 12. Photocatalytic degradation pathway of RR 120 dye under UV-A light with Sr-ZnO.

derivative, and a secondary species referred to as compound **1**. **IIP 1** subsequently broke down through cleavage of a phenyl-carbon-nitrogen (Ph–C–N) bond, leading to the formation of 2,8-diaminonaphthalene-1,3,6-triol (**IIP 2**) and compound **II**. Meanwhile, compound **1** underwent further azo bond scission, generating 6-chloro-1,3,5-triazine-2,4-diamine (**IIP 3**) and compound **III**. Compound **IV** emerged via partial amine removal and dihydroxylation of **IIP 2**, while compound **V** was derived from compound **II** and also from IIP **3**. Similarly, compound **VI** resulted from the transformation of compound **III**, involving similar deamination and hydroxylation steps. Ultimately, the advanced degradation products (compounds **IV, V, and VI**) experienced oxidative breakdown processes, culminating in complete mineralization. This final stage yielded non-toxic end products such as carbon dioxide (CO_2), water (H_2O), and trace inorganic acids evidence of thorough detoxification. Overall, the proposed degradation pathway highlights the efficacy of Sr-ZnO as a visible-light-active photocatalyst. It not only facilitates the stepwise degradation of complex azo dye molecules but also ensures the conversion of hazardous intermediates into environmentally benign final products.

4.5. *Degradation mechanism of RR 120 with Sr-ZnO*

Upon exposure to UV-A or solar irradiation, Sr-doped ZnO absorbs photons that excite electrons from the valence band (VB) to the conduction band (CB), generating electron–hole pairs, as illustrated in Fig. S6 (see Supporting information). In pristine ZnO, these charge carriers rapidly recombine, which restricts its photocatalytic capability. The substitution of Zn^{2+} with Sr^{2+} in the crystal lattice of ZnO induces lattice strain and creates oxygen vacancies that function as electron-trapping centers. These defects effectively hinder the immediate recombination of electrons and holes, thereby prolonging their lifetimes and enhancing their involvement in redox reactions at the

photocatalyst's surface. Furthermore, Sr^{2+} doping slightly modifies the band structure of ZnO by introducing mid-gap states, resulting in a modest bandgap narrowing that improves its ability to harness visible light. Concurrently, the incorporation of dopants alters the surface characteristics leading to increased surface roughness, improved wettability, and greater surface area. These features promote better dye adsorption and stronger interfacial interaction with organic pollutants like Reactive Red 120 (RR 120), facilitating more efficient degradation. The presence of oxygen vacancies not only supports prolonged charge separation but also boosts the formation of reactive oxygen species (ROS) such as superoxide anions ($O_2^{\bullet-}$) and hydroxyl radicals ($^{\bullet}OH$). These species are highly oxidative and are instrumental in attacking and decomposing dye molecules into smaller, non-toxic substances. Collectively, Sr^{2+} doping enhances ZnO's photocatalytic efficiency under both UV-A and solar illumination by simultaneously improving photon absorption, suppressing charge recombination, increasing surface-active sites, and intensifying ROS generation culminating in the effective breakdown of RR 120 dye.

4.5.1. Antibacterial activity

Antibacterial activity describes a substance's ability to suppress or destroy bacterial growth. Metal oxide nanoparticles, particularly zinc oxide (ZnO), have recently received a lot of attention due to their antibacterial properties. ZnO nanoparticles have remarkable antibacterial properties because they can produce reactive oxygen species (ROS), which can damage bacterial cell membranes, DNA, or proteins. ZnO's release of Zn^{2+} ions helps suppress microorganisms. However, loading ZnO with other elements can improve its efficiency even further. Strontium (Sr) loading has been investigated to improve ZnO's photocatalytic and antibacterial properties, resulting in improved bacterial inhibition even at low concentrations. Pure ZnO and 3 wt% Sr-loaded ZnO were tested for antibacterial activity against four common bacterial strains: *Staphylococcus aureus* (*S. aureus*), *Pseudomonas aeruginosa (P. aeruginosa*), *Bacillus subtilis (B. subtilis),* and *Escherichia coli* (Fig. S7). The antibacterial activity of these photocatalysts was evaluated by measuring the zone of inhibition (mm) at varied doses (60, 80, and 100 μg/mL) (Table 1). Results were compared to a control (aqueous solution) and a conventional antibiotic (10 μL/disc). The results show that pure ZnO has moderate antibacterial activity, with inhibition zones spanning from 1 to 7 mm for various bacterial strains and concentrations. *E. coli* and *S. aureus* were marginally more susceptible to pure ZnO than *P. aeruginosa* and *B. subtilis*. However, 3 wt% Sr-loaded ZnO showed dramatically increased antibacterial activity. At 100 μg/mL, Sr-ZnO inhibited *E. coli* up to 13 mm, whereas pure ZnO only inhibited up to 6 mm. Similarly, *S. aureus* had a maximal inhibitory zone of 11 mm with Sr-ZnO but only 7 mm with pure ZnO. Other bacteria followed a similar pattern, with inhibition zones expanding as catalyst concentrations increased. The control (aqueous solution) exhibited no inhibition, indicating that the antibacterial effects were primarily due to ZnO and Sr-ZnO. The typical antibiotic, amoxicillin, has the largest inhibition zones, spanning from 7 to 14 mm, showing its strong antibacterial characteristics. Nonetheless, the Sr-ZnO sample exhibited inhibitory zones similar to those of amoxicillin, notably for *E. coli* and *S. aureus*, showing increased antibacterial activity. This enhancement can be ascribed to Sr-ZnO's improved catalytic activity, which enhances ROS production, resulting in more bacterial damage. Finally, the study found that Sr loading considerably improves the antibacterial efficacy of ZnO nanoparticles. Sr-ZnO's enlarged inhibitory zones suggest that it could be a useful antibacterial agent with uses in healthcare, water treatment, and antimicrobial coatings. Further research could look at the processes underlying the increased activity and its long-term stability for practical application.

Table 1
Antibacterial activity of pure ZnO, 3 wt% Sr -ZnO catalysts.

Samples	Organisms	Concentrations (μg/mL) and Zone of inhibition (mm)				
		60	80	100	Control (Aqueous) 10 μL/disc	Antibacterial Standard (std) (Amoxicillin) 10 μL/disc
Bare ZnO	***S. aureus***	3	5	7	0	12
	P. aeruginosa	2	3	5	0	8
	B. subtilis	1	2	3	0	7
	E. coli	2	3	6	0	11
3 wt% Sr-ZnO	***S. aureus***	7	9	11	0	13
	P. aeruginosa	5	6	9	0	10
	B. subtilis	6	7	8	0	9
	E. coli	7	10	13	0	14

Table 2 summarises a comparison of the photocatalytic performance of Sr-loaded ZnO with other reported strontium-modified materials, emphasising the efficacy of the current photocatalyst system. In this investigation, 3 wt% Sr-loaded ZnO displayed superior degradation efficiency, removing over 100 % of RR 120 dye (50 ppm) under UV-A light in 70 min with a catalyst dosage of only 20 mg per 100 mL at neutral pH. This finding establishes the synthesised material's better activity when compared to previous research using similar catalysts under different settings. For example, under a 400 W mercury lamp, Sr-loaded ZnO degraded malachite green (MG, 20 ppm) with 84.8 % efficiency in 30 min [48], while another study using solar irradiation achieved 89.62 wt% and 94.67 % degradation of methylene blue (MB, 4 ppm) and rose bengal (RB, 3 ppm), respectively, over extended periods of 300 and 240 min [49]. A system using Sr-loaded ZnO and H_2O_2 under UV radiation demonstrated 78 % degradation of AV-17 dye (20 ppm) in 140 min [24], suggesting the need for additional oxidants. The use of Sr^{2+}-ZnO under visible light resulted in 100 % degradation of MB in 25 min [25], but the dye system and circumstances were different. Another important result revealed 99 % degradation of MB (100 ppm) in 60 min under sun irradiation with a 10 mg dose [26]. In comparison to earlier investigations, the current work shows good photocatalytic performance at a greater pollutant concentration and a moderate catalyst dosage, without the requirement for auxiliary reagents. Incorporating Sr^{2+} into ZnO improves its electrical characteristics, resulting in greater charge separation and reactive species formation. This reinforces the potential of 3 wt% Sr-ZnO as a highly efficient and reusable photocatalyst for practical environmental remediation applications. Thus, our results demonstrate both higher efficiency and shorter reaction time at comparable or lower catalyst dosages.

5. Conclusions

In this study, pure and strontium-loaded ZnO (Sr-ZnO) nanoparticles were effectively synthesised using a simple co-precipitation approach and extensively characterised for structural, morphological, optical, photocatalytic, and antibacterial properties. XRD, FT-IR, Raman, PL, UV-DRS, SEM, TEM, EDS, and XPS investigations verified the effective integration of Sr^{2+} into the ZnO lattice without affecting its wurtzite structure. Sr loading caused lattice defects, altered band gaps, enhanced charge carrier separation, and increased surface area, all of which helped to increase photocatalytic activity. Among the investigated compounds, 3 wt% Sr-ZnO performed best, attaining nearly complete degradation (≈100 %) of the Reactive Red 120 (RR 120) dye in 30 min under UV-A light and ≈ 100 % under natural sunshine in 50 min. The Sr-ZnO photocatalyst synthesized in this work outperforms previously reported ZnO-based materials in degradation efficiency, owing to the controlled Sr doping and refined particle morphology. The improved performance was due to higher visible light absorption, reactive oxygen species (ROS) production, and effective electron-hole recombination suppression. Photocatalytic tests with various pH and catalyst dosages revealed that neutral pH and 50 mg catalyst loading were the best settings. Furthermore, reusability experiments revealed the catalyst's long-

Table 2
Comparison of the dye degradation efficiency of Sr-ZnO photocatalyst with other reported strontium-modified materials.

S. No	Catalysts	Light source	Pollutants/ Concentration	Catalyst amount	Degradation (%)/time (min) & pH	Ref
1	Sr-loaded ZnO	400 W Mercury lamp	MG/ 20 ppm	2 mg/ 100 mL	≈ 84.8/30 at pH 7	[48]
2	Sr-loaded ZnO	Solar irradiation	MB/4ppm, RB/3ppm	10 mg/ 100 mL	89.62/300 at pH 7 94.67/240 at pH7	[49]
3	Sr-loaded ZnO	UV light	AV−17/ 20 ppm	0.1 g+ H_2O_2 / 100 mL	78/140 at pH 7	[24]
4	Sr^{2+}-loaded ZnO	Visible light	MB/ 50 ppm	20 mg/100 mL	≈ 100/25 at pH 7	[25]
5	Sr-loaded ZnO	Solar irradiation	MB/ 100 ppm	10 mg/ 100 mL	99/60 at pH 7	[26]
6	Sr-doped ZnO	32W-UV-A light, 365 nm & Sunlight	RR 120/ 50 ppm	50 mg/100 mL 20 mg/100 mL	≈ 100/30 at pH 7 (UV) ≈ 100/50 at pH 7 (Sunlight)	**[Present work]**

term stability and sustainability across several cycles, keeping more than 90 % efficiency. In addition to its outstanding photocatalytic activity, 3 wt% Sr-ZnO demonstrated improved antibacterial efficacy against both Gram-positive and Gram-negative bacteria, with inhibition zones comparable to standard antibiotics. The combination of photocatalytic and antibacterial properties makes Sr-loaded ZnO a promising multifunctional nanomaterial for environmental remediation, particularly in wastewater treatment and microbial control. Overall, this study demonstrates the potential of Sr-ZnO nanostructures as efficient, cost-effective, and environmentally friendly photocatalysts and antibacterial agents, stimulating further research into real-world water purification and disinfection systems.

CRediT authorship contribution statement

V. Mariyappillai: Writing – original draft, Methodology, Investigation, Data curation, Conceptualization. **C. Shiyamala:** Writing – review & editing, Supervision, Conceptualization. **M. Tiffany:** Writing – review & editing. **T. Abisheik:** Writing– review & editing, Software, Data curation. **V. Pandiyan:** Writing – review & editing. **Abdullah K. Alanazi:** Data curation, Software, Resources. **Parvathalu Kalakonda:** Writing – review & editing. **Arun Thirumurugan:** Visualization, Software. **Gabriela Sandoval-Hevia:** Validation, Software. **Krishnakumar Balu:** Writing – review & editing, Supervision, Conceptualization.

Declaration of Competing Interest

The authors declare that they have no known competing financial interests or personal relationships that could have appeared to influence the work reported in this paper.

Acknowledgments

The research was funded by Taif University, Saudi Arabia, Project No: (TU-DSPP-2024–16).

Appendix A. Supporting information

Supplementary data associated with this article can be found in the online version at doi:10.1016/j.colsurfa.2025.138212.

Data availability

Data will be made available on request.

References

[1] T. Islam, M.R. Repon, T. Islam, Z. Sarwar, M.M. Rahman, Impact of textile dyes on health and ecosystem: a review of structure, causes, and potential solutions, Environ. Sci. Pollut. Res. 30 (4) (2023) 9207–9242.
[2] S. Dutta, S. Adhikary, S. Bhattacharya, D. Roy, S. Chatterjee, A. Chakraborty, P. Rajak, Contamination of textile dyes in aquatic environment: adverse impacts on aquatic ecosystem and human health, and its management using bioremediation, J. Environ. 353 (2024) 120103.
[3] M.M. Islam, A.R. Aidid, J.N. Mohshin, H. Mondal, S. Ganguli, A.K. Chakraborty, A critical review on textile dye-containing wastewater: ecotoxicity, health risks, and remediation strategies for environmental safety, Chem. Eng. (2025) 100165.
[4] B. Lellis, C.Z. Fávaro-Polonio, J.A. Pamphile, J.C. Polonio, Effects of textile dyes on health and the environment and bioremediation potential of living organisms, Biotechnol. Res. Innov. 3 (2) (2019) 275–290.
[5] K. Ramamurthy, P.S. Priya, R. Murugan, J. Arockiaraj, Hues of risk: investigating genotoxicity and environmental impacts of azo textile dyes, Environ. Sci. Pollut. Res. 31 (23) (2024) 33190–33211.
[6] R. Al-Tohamy, S.S. Ali, F. Li, K.M. Okasha, Y.A.G. Mahmoud, T. Elsamahy, J. Sun, A critical review on the treatment of dye-containing wastewater: ecotoxicological and health concerns of textile dyes and possible remediation approaches for environmental safety, Ecotoxicol. Environ. Saf. 231 (2022) 113160.
[7] S. Sudarshan, S. Harikrishnan, G. RathiBhuvaneswari, V. Alamelu, S. Aanand, A. Rajasekar, M. Govarthanan, Impact of textile dyes on human health and bioremediation of textile industry effluent using microorganisms: current status and future prospects, Appl. Microbiol. 134 (2) (2023) lxac064.
[8] S. Dutta, S. Adhikary, S. Bhattacharya, D. Roy, S. Chatterjee, A. Chakraborty, P. Rajak, Contamination of textile dyes in aquatic environment: adverse impacts on aquatic ecosystem and human health, and its management using bioremediation, J. Environ. 353 (2024) 120103.
[9] K.M. Lee, C.W. Lai, K.S. Ngai, J.C. Juan, Recent developments of zinc oxide based photocatalyst in water treatment technology: a review, Water Res. 88 (2016) 428–448.
[10] Y. Sun, W. Zhang, Q. Li, H. Liu, X. Wang, X, Preparations and applications of zinc oxide based photocatalytic materials, Sens. Mater. 2 (3) (2023) 100069.
[11] S. Abou Zeid, Y. Leprince-Wang, Advancements in ZnO-based photocatalysts for water treatment: a comprehensive review, J. Cryst. Growth 14 (7) (2024) 611.
[12] O.D. Maynez-Navarro, J.L. Sánchez-Salas, Focus on zinc oxide as a photocatalytic material for water treatment, Int. J. Bioremediat. Biodegrad. 106 (10) (2018) 29011.
[13] K. Takahashi, A. Yoshikawa, A. Sandhu, A, Wide bandgap semiconductors, Verlag, Berlin Heidelberg, 2007.
[14] A.B. Djurišić, Y.H. Leung, Optical properties of ZnO nanostructures, Small 2 (8-9) (2006) 944–961.
[15] N. Yahya, M. Kashif, M.N. Akhtar, N. Nasir, N. Yahya, N, Versatility of ZnO nanostructures, Carbon Oxide Nanostruct. Synth. Charact. Appl. (2011) 219–244.
[16] R. Ullah, J. Dutta, Photocatalytic degradation of organic dyes with manganese-doped ZnO nanoparticles, J. Hazard. Mater. 156 (1-3) (2008) 194–200.
[17] C.B. Ong, L.Y. Ng, A.W. Mohammad, A review of ZnO nanoparticles as solar photocatalysts: synthesis, mechanisms and applications, Renew. Sustain. Energy Rev. 81 (2018) 536–551.
[18] W. Yu, J. Zhang, T. Peng, New insight into the enhanced photocatalytic activity of N-, C-and S-doped ZnO photocatalysts, Appl. Catal. B 181 (2016) 220–227.
[19] M.C. Uribe-López, M.C. Hidalgo-López, R. López-González, D.M. Frías-Márquez, G. Núñez-Nogueira, D. Hernández-Castillo, M.A. Alvarez-Lemus, Photocatalytic activity of ZnO nanoparticles and the role of the synthesis method on their physical and chemical properties, J. Photochem. Photobiol. A Chem. 404 (2021) 112866.
[20] M.T. Noman, N. Amor, M. Petru, Synthesis and applications of ZnO nanostructures (ZONSs): a review, Crit. Rev. Solid State Mater. Sci. 47 (2) (2022) 99–141.
[21] X. Shi, L. Wu, P. Hong, F. Teng, P. Hu, H. Fan, A review of recent advances in ZnO-based thin film photodetectors: Preparation, structure and strategies for performance enhancement, Opt. Laser Technol. 191 (2025) 113352.
[22] H.H. Azeez, A.A. Barzinjy, S.M. Hamad, Structure, Synthesis and Applications of ZnO Nanoparticles: A Review, Jordan J. Phys. 13 (2) (2020) 123–135.
[23] A.R. Bhapkar, S. Bhame, A review on ZnO and its modifications for photocatalytic degradation of prominent textile effluents: synthesis, mechanisms, and future directions, J. Environ. Chem. Eng. (2024) 112553.
[24] F.A. Jan, R. Ullah, U. Shah, M. Saleem, N. Ullah, N, Band gap tuning of zinc oxide nanoparticles by the addition of (1-4%) strontium. Synthesis, characterization of

the catalyst and its use for the photocatalytic degradation of acid violet-17 dye in aqueous solution, Environ. Eng. Manag. J. 19 (11) (2020).
[25] N.N. Kumaran, K. Muraleedharan, K, Photocatalytic activity of ZnO and Sr^{2+} doped ZnO nanoparticles, J. Water Proc. Eng. 17 (2017) 264–270.
[26] P. Agale, V. Salve, S. Mardikar, S. Patange, P. More, Synthesis and characterization of hierarchical Sr-doped ZnO hexagonal nanodisks as an efficient photocatalyst for the degradation of methylene blue dye under sunlight irradiation, Appl. Surf. Sci. 672 (2024) 160795.
[27] D. Bhardwaj, D. Prasher, A. Dubey, V. Dhiman, R. Tomar, One step sonochemical synthesis of single-phase Sr-doped ZnO, SN Appl. Sci. (2021) 1–7.
[28] M. Suganya, S. Anitha, D. Prabha, S. Balamurugan, J. Srivind, A.R. Balu, Enhanced photocatalytic and antifungal properties of Sr-doped PbS nanopowders, Mater. Technol. 33 (3) (2018) 214–219.
[29] S. Salvi, P. Lokhande, H. Mujawar, Photodegradation of rhodamine 6G dye by cd, sr doped ZnO photocatalyst, synthesized by mechanochemical method (ICCASP 2016). Int. Conf. Commun. Signal Process, Atlantis Press, 2016, pp. 48–53 (ICCASP 2016).
[30] G. Anandhakumari, P. Jayabal, A. Balasankar, S. Ramasundaram, T.H. Oh, K. Aruchamy, V. Polisetti, Synthesis of strontium oxide-zinc oxide nanocomposites by Co-precipitation method and its application for degradation of malachite Green dye under direct sunlight, Heliyon 9 (10) (2023).
[31] S.L. Perumal, P. Hemalatha, M. Alagara, K.N. Pandiyaraj, Investigation of structural, optical and photocatalytic properties of sr doped zno nanoparticles, Int. J. Phys. Sci. 4 (2015) 1–13.
[32] S. Harish, M. Sabarinathan, J. Archana, M. Navaneethan, K.D. Nisha, S. Ponnusamy, Y. Hayakawa, Y, Synthesis of ZnO/SrO nanocomposites for enhanced photocatalytic activity under visible light irradiation, Appl. Surf. Sci. 418 (2017) 147–155.
[33] M. Shkir, B.M. Al-Shehri, M.P. Pachamuthu, A. Khan, K.V. Chandekar, S. AlFaify, M.S. Hamdy, A remarkable improvement in photocatalytic activity of ZnO nanoparticles through sr doping synthesized by one pot flash combustion technique for water treatments, Colloids Surf. A 587 (2020) 124340.
[34] T.A. Vijayan, R. Chandramohan, S. Valanarasu, J. Thirumalai, S.P. Subramanian, Comparative investigation on nanocrystal structure, optical, and electrical properties of ZnO and Sr-doped ZnO thin films using chemical bath deposition method, J. Mater. Sci. 43 (6) (2008) 1776–1782.
[35] M.H. Mohamed, T.M. Elmorsi, H.M. Abdelbary, Enhanced adsorption of anionic dyes using Sr-doped zno nanoparticles: nonlinear kinetics and isotherm studies, AlAzhar Bull. Sci. Basic Sci. Sect. 34 (3) (2023) 2.
[36] S.I. Shanthi, S. Poovaragan, M.V. Arularasu, S. Nithya, R. Sundaram, C. M. Magdalane, M. Maaza, Optical, magnetic and photocatalytic activity studies of li, mg and sr doped and undoped zinc oxide nanoparticles, Nanosci. Nanotechnol. 18 (8) (2018) 5441–5447.
[37] R. Yousefi, F. Jamali-Sheini, M. Cheraghizade, S. Khosravi-Gandomani, A. Saaedi, N.M. Huang, M. Azarang, Enhanced visible-light photocatalytic activity of strontium-doped zinc oxide nanoparticles, J. Mater. Sci. 32 (2015) 152–159.
[38] A.S. Javaid, W.S. Javaid, M. Adnan, M. Usman, M.A. Akram, N. Bashir, N. Arshad, Synthesis and characterization of efficient Sr-doped ZnO nanostructures for optoelectronic, and photocatalytic applications, Inorg. Chem. Commun. 162 (2024) 112175.
[39] K.P. Raj, K. Sadaiyandi, A. Kennedy, R. Thamizselvi, Structural, optical, photoluminescence and photocatalytic assessment of Sr-doped ZnO nanoparticles, Mater. Chem. 183 (2016) 24–36.
[40] M. Irfan, S. Afzal, M. Hussain, M.Y. Naz, S. Shukrullah, S. Rahman, A.A.J. Ghanim, Testing of Sr-doped ZnO/CNT photocatalysts for hydrogen evolution from water splitting under atmospheric dielectric barrier plasma exposure, ACS Omega 8 (21) (2023) 18891–18900.
[41] V. Mariyappillai, C. Shiyamala, T. Abisheik, M. Tiffany, V. Pandiyan, A. Senthilraja, K. Balu, Zr-modified ZnO nanoparticles: optimized photocatalytic degradation and antibacterial efficiency for pollution control, Ceram. Int. (2025).
[42] V.D.M.Z. Barbarić-Mikočević, K. Itrić, K, Kubelka-Munk theory in describing optical properties of paper (I), Tech. Gaz. 18 (1) (2011) 117–124.
[43] M. Basseem, A.A. Emam, F.H. Kamal, A.M. Gamal, S.A. Abo Faraha, Novel functionalized of ZnO with Sm^{3+}, La^{3+}, and Sr^{2+}/ZnO single and tri-doped nanomaterials for photocatalytic degradation: synthesis, DFT, kinetics, J. Mater. Sci. 58 (33) (2023) 13346–13372.
[44] M. Yarahmadi, H. Maleki-Ghaleh, M.E. Mehr, Z. Dargahi, F. Rasouli, M.H. Siadati, Synthesis and characterization of Sr-doped ZnO nanoparticles for photocatalytic applications, J. Alloy. Compd. 853 (2021) 157000.
[45] K. Ravichandran, N. Chidambaram, T. Arun, S. Velmathi, S. Gopalakrishnan, Realizing cost-effective ZnO: sr nanoparticles@ graphene nanospreads for improved photocatalytic and antibacterial activities, RSC Adv. 6 (72) (2016) 67575–67585.
[46] F.A. Jan, R. Ullah, U. Shah, M. Saleem, N. Ullah, Band gap tuning of zinc oxide nanoparticles by the addition of (1-4%) strontium. Synthesis, characterization of the catalyst and its use for the photocatalytic degradation of acid violet-17 dye in aqueous solution, Environ. Eng. Manag. J. 19 (11) (2020).
[47] A. Joy, M.R. Viswanathan, B.K. Vijayan, C.G. Silva, I. Basheer, S. Sugathan, A. Shereef, Solar photocatalysts: non-metal (C, N, and S)-doped ZnO synthesized through an industrially sustainable in situ approach for environmental remediation applications, RSC Adv. 14 (30) (2024) 21655–21667.
[48] R. Akram, Z.M. Almohaimeed, A. Bashir, M. Ikram, K.W. Qadir, Q. Zafar, Q, Synthesis and characterization of pristine and strontium-doped zinc oxide nanoparticles for methyl Green photo-degradation application, Nanotech 33 (29) (2022) 295702.
[49] N. Mokrani, E.G. Temam, H.B. Temam, H. Barkat, M. Althamthami, Enhancing water purification with light-activated strontium-doped ZnO thin films, Adv. Nat. Sci. Nanosci. Nanotechnol. 16 (1) (2025) 015012.